文章编号:1000-0887(2016)12-1359-19

An MPS-FEM Coupled Method for the Comparative Study of Liquid Sloshing Flows Interacting With Rigid and Elastic Baffles*

ZHANG You-lin, CHEN Xiang, WAN De-cheng

(*State Key Laboratory of Ocean Engineering*(*Shanghai Jiao Tong University*);
School of Naval Architecture, Ocean & Civil Engineering, Shanghai Jiao Tong University;
Collaborative Innovation Center for Advanced Ship and Deep-Sea Exploration,
Shanghai 200240, *P.R.China*)

Abstract: Fluid-structure interaction (FSI) problems caused by fluid impact loads are commonly existent in naval architectures and ocean engineering fields. For instance, the impact loads due to non-linear fluid motion in a liquid sloshing tank potentially affect the structural safety of cargo tanks or vessels. The challenges of numerical study on FSI problems involve not only multidisciplinary features, but also accurate description of non-linear free surface. A fully Lagrangian particle-based method , the moving particle semi-implicit and finite element coupled method (MPS-FEM), is developed to numerically study the FSI problems. Taking into account the advantage of the Lagrangian method for large deformations of both fluid and solid boundaries, the MPS method is used to simulate the fluid field while the finite element method(FEM) to calculate the structure field. Besides, the partitioning strategy is employed to couple the MPS and FEM modules. To validate accuracy of the proposed algorithm, a benchmark case is numerically investigated. Both the patterns of free surface and the deflections of the elastic structures are in good agreement with the experimental data. Then, the present FSI solver is applied to the comparative study of the mitigating effects of rigid baffles and elastic baffles on the sloshing motions and impact loads.

Key words: particle method; moving particle semi-implicit (MPS); FEM; FSI; sloshing; dam break; MLParticle-SJTU solver

CLC number: O35; U663 **Document code**: A

doi: 10.21656/1000-0887.370514

Introduction

In the fields of naval architecture and ocean engineering, the phenomena corresponding to fluid-structure interactions are of significant importance. For instance, tankers or other ocean structures could be damaged by sloshing flows, slamming or green water in-

* Received 2016-11-26; Revised 2016-12-07
Project supported by the National Natural Science Foundation of China (51379125; 51490675; 11432009; 51579145; 11272120) and the Chang Jiang Scholars Program of China(T2014099)
Corresponding author, WAN De-cheng, E-mail: dcwan@sjtu.edu.cn

duced by huge waves. Therefore, special attention is devoted to the FSI problems.

In recent decades, various numerical methods have been applied to the investigations of the FSI phenomena with the development of computer science. For example, Idelsohn et al.[1] applied the so called particle finite element method (PFEM) for the simulation of the interaction between an elastic structure and free surface flows in a sloshing tank. Fossa et al.[2] investigated the possible effects of a deformable structure on the sloshing phenomenon with the ADINA software based on the finite element method for both fluid and structural analysis. Liao and Hu[3] developed a finite difference method (FDM) coupled with the finite element method to simulate the interaction between liquid sloshing flow in a rolling tank and a thin elastic plate. Paik and Carrica[4] developed a nonlinear finite element solver coupled with a URANS/DES overset grid solver. The FSI problems of rolling tanks partially filled with fluid interacting with an elastic bar clamped to the bottom or top were numerically simulated. However, applications of these grid-based approaches were restricted by the challenges, e.g. inefficient process of grid generation for complex-shape structures, requirement of dynamic mesh technologies for moving boundary or large structural deformation and simulation of free surface with large deformation or breaking, etc.

In recent years, the Lagrangian meshless method, as a new-generation computational method for the analysis of fluid mechanics, was promising for these challenges and drew special attentions from the researchers. One representative meshless particle method for free surface flow is the MPS method which was originally proposed by Koshizuka and Oka[5] for incompressible flows. Since kinds of improvements were proposed to suppress the numerical unphysical pressure oscillation[6-12], the MPS method could be introduced to FSI problems. For instance, Mitsume et al.[13-14] proposed an improved MPS-FE coupled method with a polygon wall boundary model. Hwang et al.[15-16] developed a fully Lagrangian MPS-based coupled method and applied the solver to dam break and violent sloshing flow with elastic structures. Sun et al.[17] developed a modified MPS method coupled with the FEM method for the 2D fluid-structure interaction problem, such as violent flow impacting onto a flexible structure.

Additionally, both accuracy and efficiency of the numerical study of FSI problems are involved with the coupling strategies between fluid solvers and structural solvers. Generally, the coupling strategies can be classified into 2 groups, the monolithic and the partitioned coupling approaches. For the monolithic coupling approach, a single system equation involving all variables related to both the fluid and structure dynamics is solved simultaneously[18]. However, the equation is of much difficulty to form without any modification of complicated engineering problems[19] and is expensive to be solved[20]. On the contrary, the fluid and structure fields are self-governed by different equations and solved separately for the partitioned coupling approach. The interfacial information is communicated explicitly between the fluid and structural solvers. This approach allows the use of separate fluid and structure codes or established software for each computational domain[3]. In view of these advantages, the partitioned coupling approach is utilized in this paper.

The main aim of this study is to develop a MPS-FEM coupled method and validate the capability of the proposed method for FSI problems. Firstly, a fully Lagrangian FSI solver is implemented by extending the in-house MPS solver MLParticle-SJTU[21-25] with the FEM method for structure analysis. The methods for fluid analysis, structural deformation together with the coupling strategy are introduced. Then, a benchmark case is numerically investigated. Both patterns of free surface and deflections of the elastic structures are compared against the experimental data. Finally, the present FSI solver is applied to the comparative study on the mitigating effects of rigid and elastic baffles on the sloshing motions and impact loads.

1 Numerical methods

1.1 Numerical method for fluid analysis

In this study, the fluid domain is calculated with our in-house particle solver MLParticle-SJTU based on the MPS method.

1.1.1 Governing equations

Governing equations for incompressible viscous fluid in the Lagrangian system are

$$\nabla \cdot \boldsymbol{V} = 0, \tag{1}$$

$$\frac{\mathrm{D}\boldsymbol{V}}{\mathrm{D}t} = -\frac{1}{\rho}\nabla P + \nu \nabla^2 \boldsymbol{V} + \boldsymbol{g}, \tag{2}$$

where $\boldsymbol{V}$ is the velocity vector, t is time, ρ is the fluid density, P is pressure, ν is the kinematic viscosity, $\boldsymbol{g}$ is the gravity acceleration.

1.1.2 Kernel function

In the particle method, governing equations are expressed with the particle interaction models and based on the kernel function[26]

$$W(r) = \begin{cases} \dfrac{r_e}{0.85r + 0.15r_e} - 1, & 0 \leqslant r < r_e, \\ 0, & r_e \leqslant r, \end{cases} \tag{3}$$

where r is the distance between particles and r_e is the effect radius.

1.1.3 Discrete expressions of particle interaction models

The particle interaction models, including the differential operators of gradients and being divergent and Laplacian, are defined as

$$\langle \nabla \phi \rangle_i = \frac{d}{n^0} \sum_{j \neq i} \frac{\phi_j + \phi_i}{| \boldsymbol{r}_j - \boldsymbol{r}_i |^2} (\boldsymbol{r}_j - \boldsymbol{r}_i) \cdot W(| \boldsymbol{r}_j - \boldsymbol{r}_i |), \tag{4}$$

$$\langle \nabla \cdot \boldsymbol{\Phi} \rangle_i = \frac{d}{n^0} \sum_{j \neq i} \frac{(\boldsymbol{\Phi}_j - \boldsymbol{\Phi}_i) \cdot (\boldsymbol{r}_j - \boldsymbol{r}_i)}{| \boldsymbol{r}_j - \boldsymbol{r}_i |^2} W(| \boldsymbol{r}_j - \boldsymbol{r}_i |), \tag{5}$$

$$\langle \nabla^2 \phi \rangle_i = \frac{2d}{n^0 \lambda} \sum_{j \neq i} (\phi_j - \phi_i) \cdot W(| \boldsymbol{r}_j - \boldsymbol{r}_i |), \tag{6}$$

where ϕ is an arbitrary scalar function, $\boldsymbol{\Phi}$ is an arbitrary vector, d is the number of space dimensions, n^0 is the initial particle number density for incompressible flow, λ is a parameter and defined as

$$\lambda = \frac{\sum_{j \neq i} W(|\boldsymbol{r}_j - \boldsymbol{r}_i|) \cdot |\boldsymbol{r}_j - \boldsymbol{r}_i|^2}{\sum_{j \neq i} W(|\boldsymbol{r}_j - \boldsymbol{r}_i|)}, \tag{7}$$

which is introduced to keep the variance increase equal to that of the analytical solution[27]

$$\lambda = \int_V W(\boldsymbol{r}) \cdot \boldsymbol{r}^2 \mathrm{d}V \Big/ \int_V W(\boldsymbol{r}) \mathrm{d}V. \tag{8}$$

1.1.4 Model for incompressibility

The incompressible condition for the MPS method is represented by keeping the particle number density constant. In each time step, there are 2 stages: first, the temporal velocity of particles is calculated based on viscous and gravitational forces, and particles move according to the temporal velocity; second, pressure is implicitly calculated by solving Poisson's equation, and the velocity and particle position are updated according to the obtained pressure. The pressure Poisson's equation (PPE) in the present MPS solver is defined as

$$\langle \nabla^2 P^{n+1} \rangle_i = (1 - \gamma) \frac{\rho}{\Delta t} \nabla \cdot \boldsymbol{V}_i^* - \gamma \frac{\rho}{\Delta t^2} \frac{\langle n^* \rangle_i - n^0}{n^0}, \tag{9}$$

where γ is a blending parameter with a value between 0 and 1. The range of $0.01 \leqslant \gamma \leqslant 0.05$ is better according to numerical experiments conducted by Lee et al.[28]. In this paper, $\gamma = 0.01$ for all simulations.

1.1.5 Free surface particle detection method

For the MPS method, pressure in the fluid domain will be closely affected by the accuracy of free surface detection. In the present solver, we employ a free surface detection method proposed by Zhang et al.[26]

$$\langle \boldsymbol{F} \rangle_i = \frac{d}{n^0} \sum_{j \neq i} \frac{1}{|\boldsymbol{r}_i - \boldsymbol{r}_j|} (\boldsymbol{r}_i - \boldsymbol{r}_j) W(\boldsymbol{r}_{ij}), \tag{10}$$

where vector function $\boldsymbol{F}$ represents the asymmetry of arrangements of neighboring particles. Particles satisfying

$$\langle |\boldsymbol{F}| \rangle_i > 0.9 |\boldsymbol{F}|^0 \tag{11}$$

are considered as free surface particles, where $|\boldsymbol{F}|^0$ is the initial value of $|\boldsymbol{F}|$ for surface particles.

1.2 Numerical method for structure analysis

According to the FEM theory, the spatially discretized structural dynamic equations governing the motion of structural elements, can be expressed as

$$\boldsymbol{M}\ddot{\boldsymbol{y}} + \boldsymbol{C}\dot{\boldsymbol{y}} + \boldsymbol{K}\boldsymbol{y} = \boldsymbol{F}(t), \tag{12}$$

$$\boldsymbol{C} = \alpha_1 \boldsymbol{M} + \alpha_2 \boldsymbol{K}, \tag{13}$$

where $\boldsymbol{M}$, $\boldsymbol{C}$, $\boldsymbol{K}$ are the mass matrix, the Rayleigh damping matrix and the stiffness matrix of the structure, respectively. $\boldsymbol{F}$ is the external force vector acting on the structure and varies with the computational time. $\boldsymbol{y}$ is the displacement vector of the structure. α_1 and α_2 are coefficients related to natural frequencies and damping ratios of the structure.

To solve the structural dynamic equations, another 2 set of functions should be introduced to set up a closed-form equation system. Here, Taylor's expansions of velocity and displacement developed by Newmark[29] are employed:

$$\dot{\boldsymbol{y}}_{t+\Delta t_s} = \dot{\boldsymbol{y}}_t + (1-\gamma)\ddot{\boldsymbol{y}}_t \Delta t_s + \gamma \ddot{\boldsymbol{y}}_{t+\Delta t_s} \Delta t_s, \qquad 0 < \gamma < 1, \tag{14}$$

$$\boldsymbol{y}_{t+\Delta t_s} = \boldsymbol{y}_t + \dot{\boldsymbol{y}}_t \Delta t_s + \frac{1-2\beta}{2} \ddot{\boldsymbol{y}}_t \Delta t_s^2 + \beta \ddot{\boldsymbol{y}}_{t+\Delta t_s} \Delta t_s^2, \qquad 0 < \beta < 1, \tag{15}$$

where β and γ are important parameters of the Newmark-β method, and set to $\beta = 0.25$, $\gamma = 0.5$ for all simulations in the present paper. The structural time step size is represented by Δt_s. From eqs. (12) ~ (15), the displacement at $t = t + \Delta t_s$ can be solved with the following formulas[30]

$$\bar{\boldsymbol{K}} \boldsymbol{y}_{t+\Delta t_s} = \bar{\boldsymbol{F}}_{t+\Delta t_s}, \tag{16a}$$

$$\bar{\boldsymbol{K}} = \boldsymbol{K} + a_0 \boldsymbol{M} + a_1 \boldsymbol{C}, \tag{16b}$$

$$\bar{\boldsymbol{F}}_{t+\Delta t_s} = \boldsymbol{F}_t + \boldsymbol{M}(a_0 \boldsymbol{y}_t + a_2 \dot{\boldsymbol{y}}_t + a_3 \ddot{\boldsymbol{y}}_t) + \boldsymbol{C}(a_1 \boldsymbol{y}_t + a_4 \dot{\boldsymbol{y}}_t + a_5 \ddot{\boldsymbol{y}}_t), \tag{16c}$$

$$\begin{cases} a_0 = \dfrac{1}{\beta \Delta t_s^2}, \ a_1 = \dfrac{\gamma}{\beta \Delta t_s}, \ a_2 = \dfrac{1}{\beta \Delta t_s}, \ a_3 = \dfrac{1}{2\beta} - 1, \ a_4 = \dfrac{\gamma}{\beta} - 1, \\ a_5 = \dfrac{\Delta t_s}{2}\left(\dfrac{\gamma}{\beta} - 2\right), \ a_6 = \Delta t_s (1-\gamma), \ a_7 = \gamma \Delta t_s, \end{cases} \tag{16d}$$

where $\bar{\boldsymbol{K}}$ and $\bar{\boldsymbol{F}}$ are the so-called effective stiffness matrix and the effective force vector, respectively. Finally, the accelerations and velocities corresponding to the next time step are updated as follow:

$$\ddot{\boldsymbol{y}}_{t+\Delta t_s} = a_0(\boldsymbol{y}_{t+\Delta t_s} - \boldsymbol{y}_t) - a_2 \dot{\boldsymbol{y}}_t - a_3 \ddot{\boldsymbol{y}}_t, \tag{17}$$

$$\dot{\boldsymbol{y}}_{t+\Delta t_s} = \dot{\boldsymbol{y}}_t + a_6 \ddot{\boldsymbol{y}}_t + a_7 \ddot{\boldsymbol{y}}_{t+\Delta t_s}. \tag{18}$$

1.3 Coupling strategy for FSI problems

In the present study, the partitioned coupling strategy between the MPS and the FEM is implemented in the FSI solver since it has the advantages of code modularity and flexibility to enhance the computational accuracy and efficiency. For the development of a partition-based FSI solver, the appropriateness and preciseness of its fluid-structure coupling system is one of the crucial issues[15].

The concepts of the present coupling system is shown in fig. 1. The main feature of this strategy corresponds to the different sizes of time steps in fluid and structure analysis. According to the Courant-Friedrichs-Lewy (CFL) condition, fluid time step size Δt_f is commonly set to a much small value. Correspondingly, a much larger structural time step size Δt_s would be utilized in the present strategy to improve the calculation efficiency since the Newmark-β method, which is suitable for structure analysis, is an implicit approach. Here, Δt_s is a k multiple of Δt_f, where k is an integer. In each cycle of FSI simulation, the fluid analysis is performed based on the MPS solver from time step t_{n+1} to t_{n+k} firstly. Mean pressures of particles on the fluid-structure interface are calculated as

$$\bar{p}_{n+k} = \frac{1}{k} \sum_{i=1}^{k} p_{n+i}, \tag{19}$$

where p_{n+i} is the fluid particle pressure on the wall boundary at instant $t_n + i\Delta t_f$. For the structure analysis, the external force is calculated based on average pressure $\bar{p}_{n+1}$ acting on the structure surface and the FEM solver is applied at time step t_{n+k}. After structure analysis, the position and velocity of structure particles are updated and considered as new boundary conditions for the calculation of fluid physical variables in the next time step. Remarkably, the positions of particles should be updated within time steps t_{n+1} and t_{n+k-1} based on the velocities of particles calculated in time step t_n to avoid the instability of fluid field caused by the large displacements of structure particles within Δt_s.

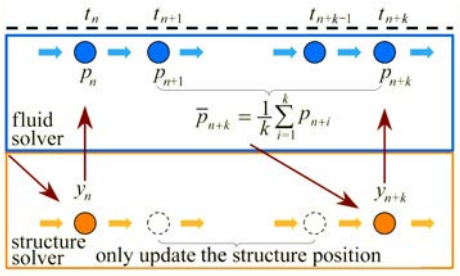

Fig. 1 The concept of the coupling strategy

1.4 Data exchange on the fluid-structure interface

In the present paper, 2D FSI problems are considered and the structures will be discretized to beam elements for the structural physics. As a result, special treatments need to be applied for data exchange on the fluid-structure interface, including the application of external force onto the beam nodes and the deformation of the structural particle model corresponding to the displacements of beam elements. Here, a particle group scheme is considered[16]. Structural particles located within the same section are grouped. For the force exchange, the concept for the numerical considerations is shown in fig. 2. Herein, the vector $\boldsymbol{F}_{Gi,l}$ and $\boldsymbol{F}_{Gi,r}$ represent the force acting on left and right boundary particle of the structural group i, respectively. As mentioned previously, the pressure of boundary particles is calculated with the MPS method initially. Then, force acting on the structural boundary particle within the structural group is calculated by the integration of average pressure acting on the interface. After this, the resultant of forces on particles within the same group will acting onto the structural FEM node as the external load for the structural analysis. For the deformation of the structural particle model, particles within a group move as one body based on the nodal linear velocities u_i and v_i which represent the velocities of beam nodes. Then, the final position of structure particles can be updated according to the rotation of the group around the center of the section based on angular velocity ω_i. The concept for the numerical considerations of the deformation of the structural particle model is shown in fig. 3.

1.5 Particle interaction model

In the numerical process of fluid-structure interaction, position of fluid particles will be updated corresponding to the structure deformation which is predicted by the FEM mod-

ule. However, the structural particles may get much too close to the fluid particles during structure deformation, and thus, result in improper repulsive forces between particles near the interface. This phenomenon may lead to non-physical pressure fluctuations and less accurate structural deformation. To avoid the clusters of particles and obtain the proper repulsive forces especially near the interface, a special particle interaction model is built in the FSI solver.

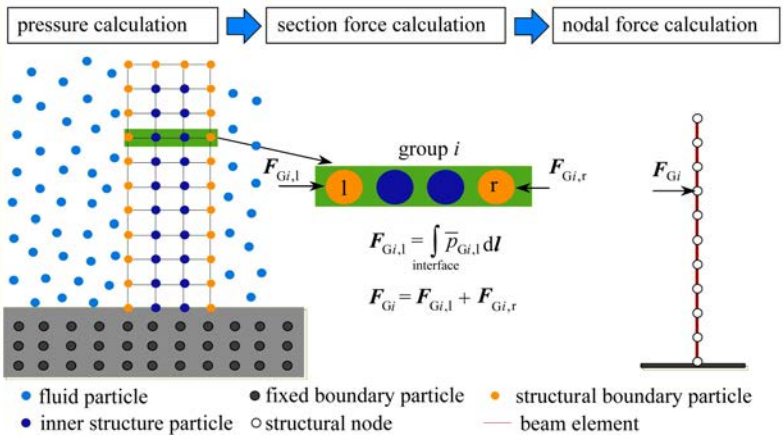

Fig. 2 The concept for the numerical considerations of fluid-structure coupling force exchange

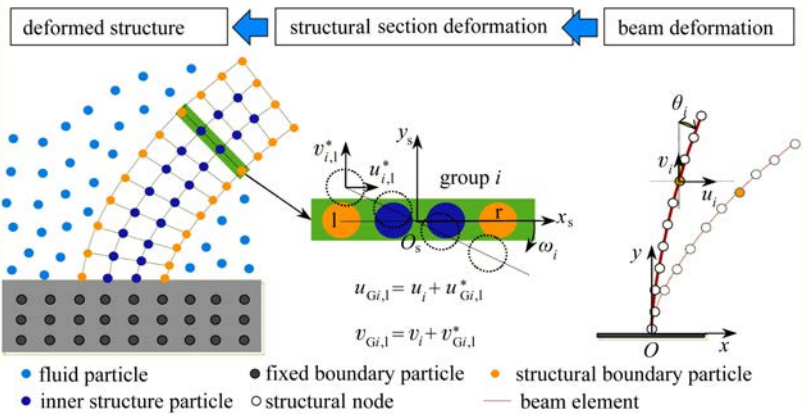

Fig. 3 The concepts for the numerical considerations of structural particle model deformation

The schematic diagram of the particle interaction model is shown in fig. 4. Before the structure deformation, the structural particles keep a proper distance from the fluid particles, as far as the positions of particles before collision. During the process of structural deformation, the structural particle moves from position s_n to s_{n+1} based on the FEM analysis while the fluid particle moves from position f_n to f^*_{n+1} based on the fluid analysis. When the distance between particles gets smaller than αl_0, the particle interaction model will work for the position correction of fluid particles. Here, l_0 denotes the initial particle spacing and α is the coefficient equal to 0.6 in this paper. According to the following formulas, the position of fluid particles is updated from position f^*_{n+1} to f_{n+1}.

$$\begin{cases} \boldsymbol{v}_{\mathrm{fs}}^{*} = \boldsymbol{v}_{\mathrm{s}} - \boldsymbol{v}_{\mathrm{f}}^{*}, \\ \boldsymbol{v}^{\mathrm{c}} = \dfrac{|\boldsymbol{v}_{\mathrm{fs}}^{*} \cdot \boldsymbol{r}_{\mathrm{fs}}^{*}|}{|\boldsymbol{r}_{\mathrm{fs}}^{*}|} \boldsymbol{r}_{\mathrm{fs}}^{*}, \\ \boldsymbol{v}_{\mathrm{f}} = \boldsymbol{v}_{\mathrm{f}}^{*} + \boldsymbol{v}^{\mathrm{c}}, \end{cases} \tag{20}$$

where $\boldsymbol{v}_{\mathrm{s}}$ denotes the velocity vector of structural particle from initial position s_n to final position s_{n+1}, $\boldsymbol{v}_{\mathrm{f}}^{*}$ and $\boldsymbol{v}_{\mathrm{f}}$ denote the velocity vectors of fluid particle from position f_n to temporary position f_{n+1}^{*} and final position f_{n+1}, respectively. $\boldsymbol{v}_{\mathrm{fs}}^{*}$ and $\boldsymbol{r}_{\mathrm{fs}}^{*}$ denote the relative velocity vector and relative position vector, $\boldsymbol{v}^{\mathrm{c}}$ denotes the velocity adjustment of fluid particle from the temporary position to the collision position.

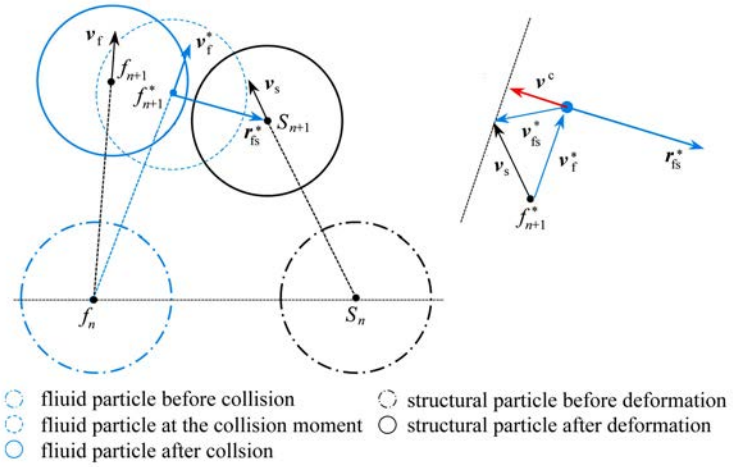

Fig. 4 Schematic diagram of the particle interaction model

2 Numerical Simulations

2.1 Validation test of FSI solver—discharged flow interacting with elastic gate

For the verification of our MPS-FEM coupled method, interaction between discharged flow and an elastic gate is numerically studied and the results are compared with their corresponding experimental and numerical data by Antoci et al.[31] in this section.

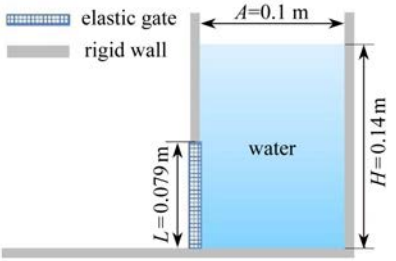

Fig. 5 Schematic view of a reservoir with an elastic gate (Antoci et al.[31])

In this numerical test, the 2D reservoir is filled with water at a level of 0.14 m and a width of 0.1 m, as shown in fig. 5. An elastic gate is installed at the lower part of the left wall of the tank, the upper end of the gate is fixed while the lower end is free to deform.

Both the fluid and structure models are discretized into particles, detailed calculation parameters are shown in table 1.

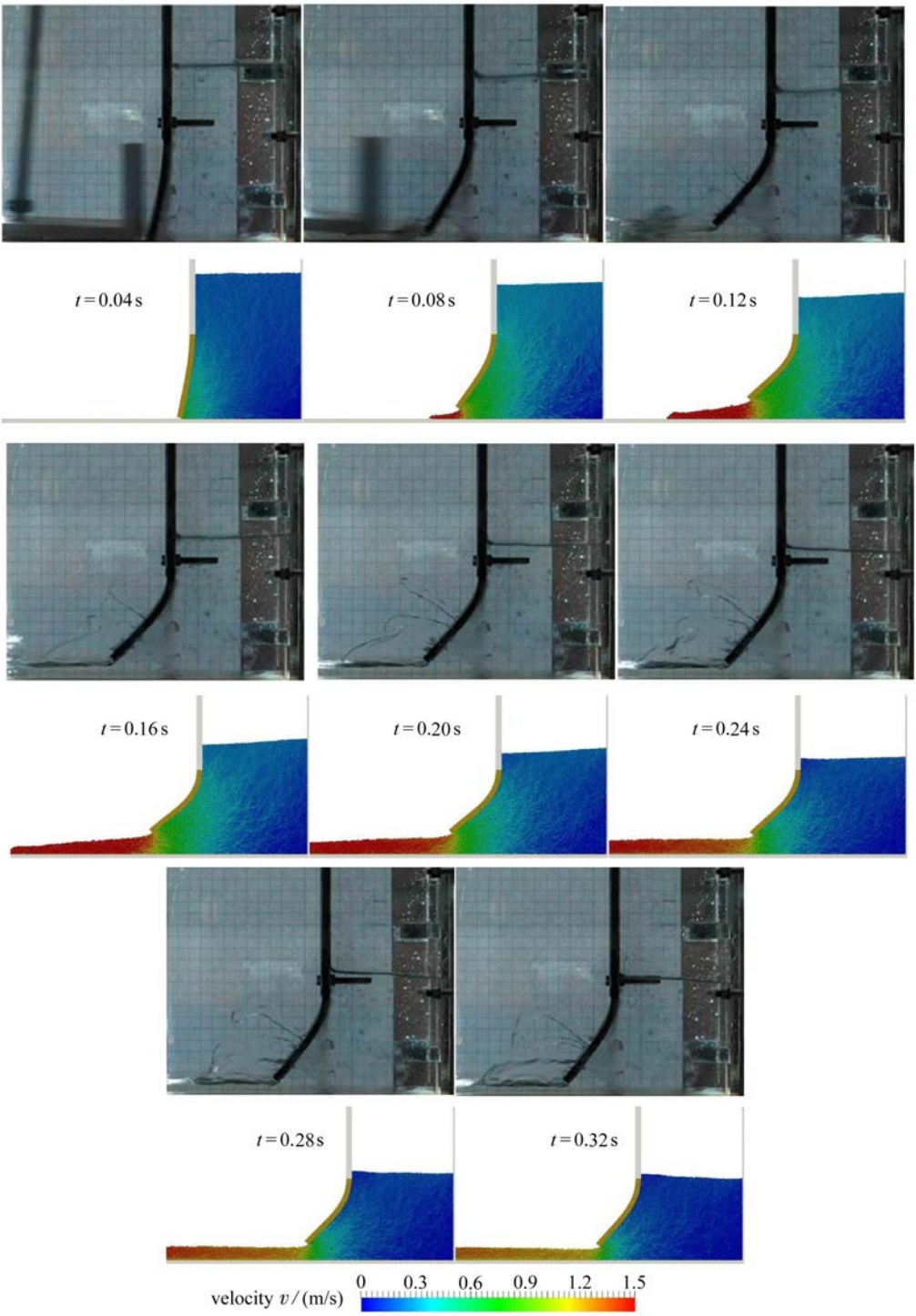

Fig. 6 Snapshots of the structural deformation and the free surface (camera shots: experimental results from Antoci et al.[31]; computer graphics: present results from the MPS-FEM)

Table 1 Parameters of the numerical test

structure parameter	value	fluid parameter	value
gate thickness τ /m	0.005	fluid density ρ_f /(kg/m^3)	1 000
structure density ρ_s /(kg/m^3)	1 100	kinematic viscosity ν /(m^2/s)	1×10^{-6}
Young's modulus E /MPa	10	gravitational acceleration g /(m/s^2)	9.81
damping coefficient α_1	0	particle spacing l_0 /m	0.001
damping coefficient α_2	0.025	total particle number n_t	16 561
time step size Δt_s /s	1×10^{-3}	time step size Δt_f /s	1×10^{-4}

Fig. 6 shows the deformation process of the elastic gate and the free surface elevation at different instants. The numerical data are compared with experimental results at the same instants with an interval of 0.04 s. It can be observed that water flow out of the reservoir immediately after the gate is pushed open by the hydrostatic pressure of stored water. During the stage $t = 0.04 \sim 0.16$ s, deformation of the gate together with the velocity of flow increases gradually, while the free surface level decreases due to the flood discharge. After instant $t = 0.16$ s, decrease of the flood velocity can be observed. Generally, profiles of the deformed baffle and the free surface are coincident with those of the experiment. In view of the comparisons of displacements at the free end of the gate shown in fig. 7 and the time histories of water levels shown in fig. 8, the structural deformation results from varying hydrodynamics can be accurately simulated by the proposed MPS-FEM coupled solver.

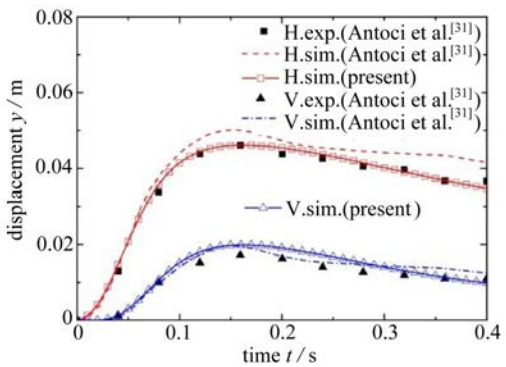

Fig. 7 Horizontal(H.) and vertical(V.) displacements at the free end of the plate

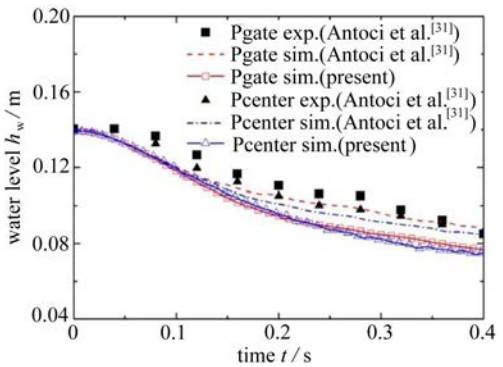

Fig. 8 Water levels just behind the gate (Pgate) and 5 cm far from it (Pcenter)

2.2 Application of FSI solver—sloshing flows interacting with rigid/elastic baffles

In the design of LNG tanker system, baffles are extensively utilized to restrain the sloshing motions and impact loads in liquid tanks. Since the liquid carrier will experience various sea states during operation, the investigation of improving effects of baffles under varying excitation frequencies is of significant practical interest. In addition, elasticity of the baffles should not be overlooked particularly for the large-scale testing or the full-scale engineering applications. With this motivation, 3 general sets of numerical simulations are conducted for the investigation on the mitigating effects of baffles on the sloshing motions and impact loads.

In this section, the geometry and filling ratio of fluid are shown in fig. 9, which are the

same with those from Idelsohn et al.[1]. The rectangular tank is set without any baffle for the first series of simulations while with a rigid baffle or an elastic baffle clamped at the rolling center for the other two series of simulations, listed as follow:

Series A: sloshing in the tank without any baffle;

Series B: sloshing in the tank with a rigid baffle;

Series C: sloshing in the tank with an elastic baffle.

The tanks are forced to roll harmonically around bottom center point O. The governing equation for the rolling motion is

$$\theta(t) = \theta_0 \sin(\omega t), \tag{21}$$

where $\theta(t)$ is the rotation angle of the tank, θ_0 is the excitation amplitude, ω is the angular frequency. The detailed fluid and structural properties and numerical conditions are listed in table 2.

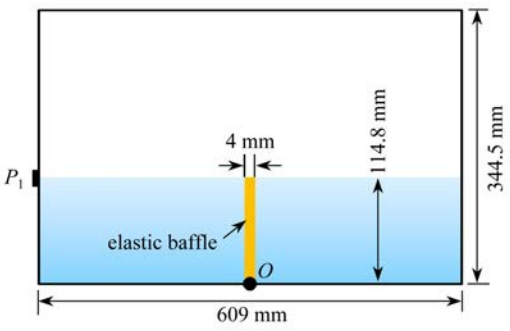

Fig. 9 Schematic diagram of the rolling tank with an elastic baffle

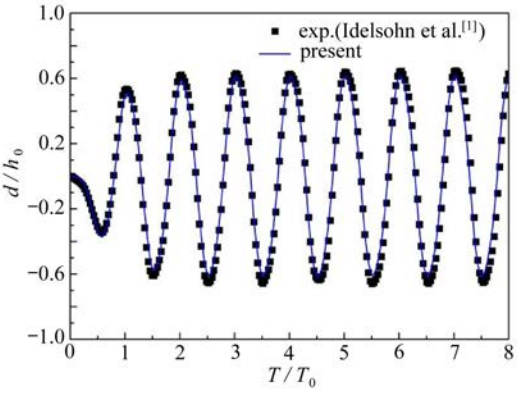

Fig. 10 Time histories of the horizontal displacements at the free end of the elastic baffle (ω/ω_0 = 1.05)

Table 2 Parameters for the numerical cases

structure parameter	value	fluid parameter	value
structure density ρ_s /(kg/m^3)	1 100	fluid density ρ_f /(kg/m^3)	917
Young's modulus E /Pa	6×10^6	kinematic viscosity ν /(m^2/s)	5×10^{-5}
length l /m	0.114	gravitational acceleration g /(m/s^2)	9.81
clamped position	bottom	fluid depth d /m	0.114
number of elements n_e	58	rolling frequency ω /(rad/s)	5.215
damping coefficient α_1	0	rolling amplitude θ_0 /(°)	4
damping coefficient α_2	0.025	particle spacing l_0 /m	0.002
time step size Δt_s /s	2×10^{-3}	time step size Δt_f /s	2×10^{-4}

To rigorously verify the reliability of the present MPS-FEM coupled method for practical FSI problems, series C with the excitation ω/ω_0 = 1.05 is simulated and compared against corresponding experimental data from Idelsohn et al.[1]. Fig. 10 shows the comparison of dimensionless time histories of the horizontal displacement at the free end of the baffle. Here, time is made dimensionless with excitation period T_0 and displacement with reference fluid depth h_0. Present numerical results are in good agreement with the experimental data in terms of both amplitude and period of the displacement.

To preliminarily investigate the mitigating effects of the rigid and elastic baffles, 2 typical frequencies, the frequency nearby (ω/ω_0 = 1.05) or far from (ω/ω_0 = 1.61) the resonant frequency, are considered as the excitation frequencies for the rolling tank.

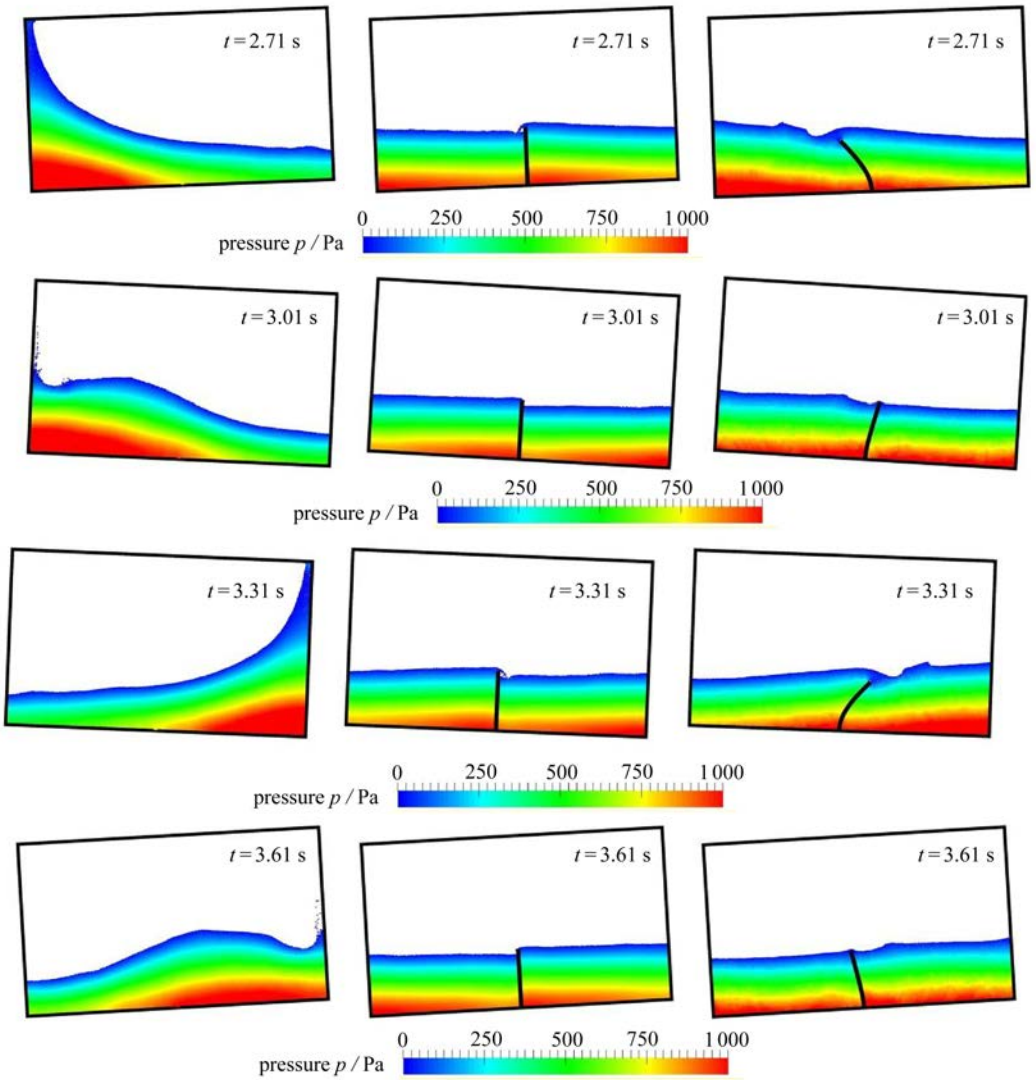

(a) Without any baffle (b) With a rigid baffle (c) With an elastic baffle

Fig. 11 Illustration of sloshing flows in the tank (ω/ω_0 = 1.05)

Fig. 11 shows the comparison between the snapshots of the 3 different cases at the same instants, with a rolling excitation at resonant frequency ω/ω_0 = 1.05. In the simulation of sloshing without any baffle, violent liquid motion exists in the tank. Within one period of rolling motion, the front of the fluid column impacts on to both sides of the tank and even climbs along the tank walls up to the ceiling. In the simulation of sloshing with a rigid baffle, the smooth free surface is observed and the motion of the liquid column is mitigated significantly. In comparison, complicated folds and overturnings of the free surface in the elastically baffled tank are observed at the tip of the elastic baffle although no impacting

phenomenon occurs inside the tank.

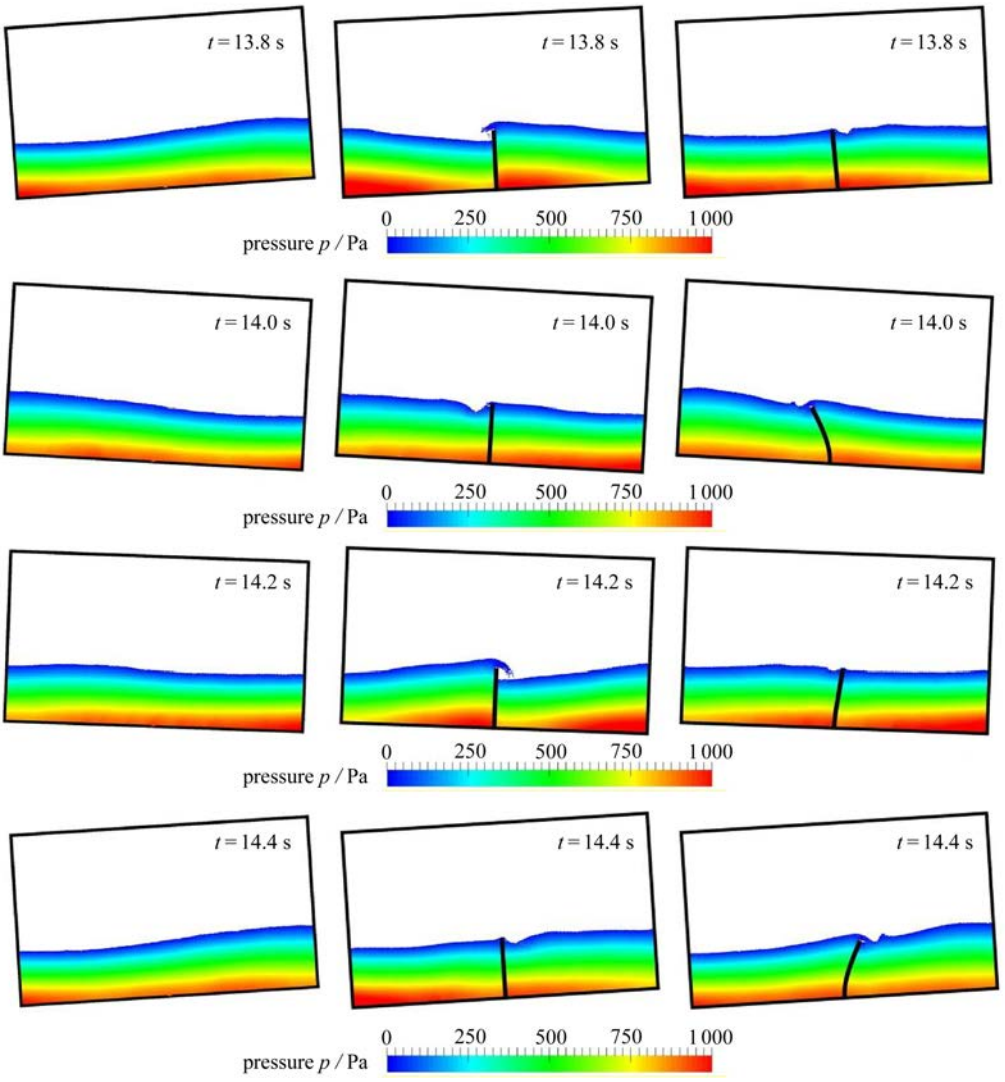

(a) Without any baffle (b) With a rigid baffle (c) With an elastic baffle

Fig. 12 Illustration of sloshing flows in the tank (ω/ω_0 = 1.61)

Fig. 12 illustrates comparison between the snapshots of the 3 different cases at the same instants, with a rolling excitation frequency ω/ω_0 = 1.61 which is far away from resonant frequency ω_0. In the case of sloshing flow in the tank without any baffle, liquid perturbation is observed in comparison with the violent liquid motion corresponding to the resonant frequency. The form of free surface approximates standing waves, as shown in fig. 12 (a). In the case with a rigid baffle, the tank is divided into 2 parts by the baffle. As the sloshing flows occur in each part independently, similar forms of free surfaces are noticed on both sides of the baffle and evident difference of fluid levels exists on both sides of the baffle, as shown in fig. 12(b). Besides, the liquid columns climb up to a higher level along the tank walls compared to that in fig. 12(a) during rolling motion of the tank. This phe-

nomenon may result from the fact that the excitation frequency is close to the resonant frequency of the tank parts. In the case with an elastic baffle shown in fig. 12(c), the difference of fluid levels nearby the two sides of the baffle is not obvious.

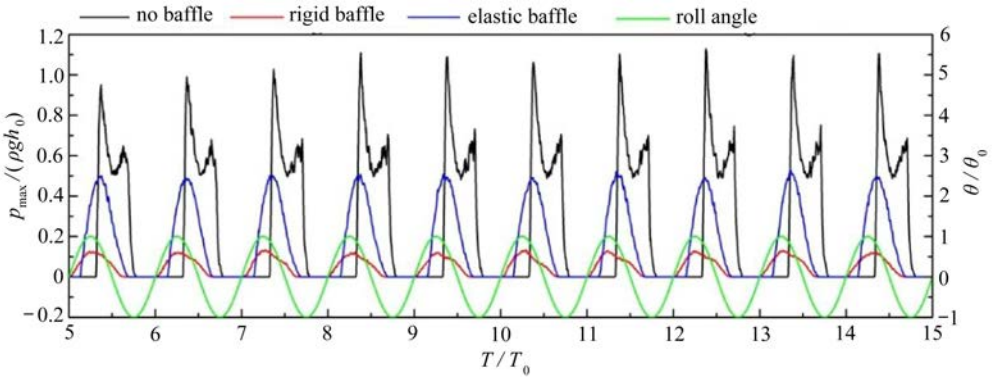

(a) $\omega/\omega_0 = 1.05$

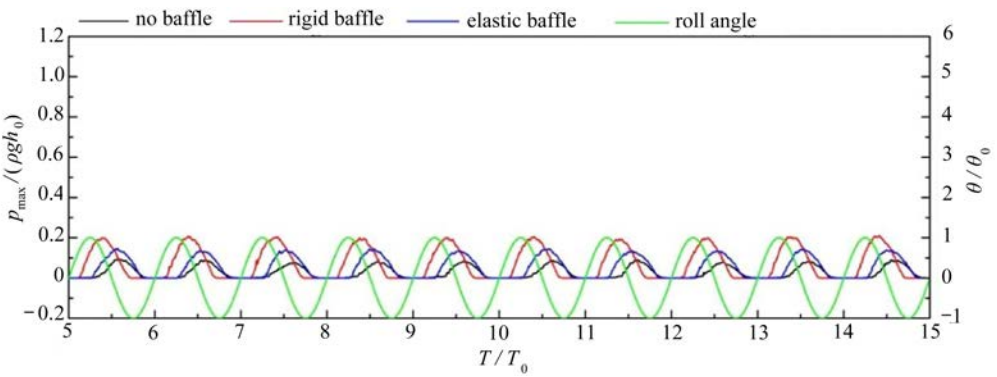

(b) $\omega/\omega_0 = 1.61$

Fig. 13 Time histories of pressures at point P_1

Fig. 13 shows the comparison of dimensionless time histories of pressures for the 3 series of simulations without any baffle, with a rigid baffle and with an elastic baffle. Here, time is been made dimensionless with excitation period T_0, pressure with hydrostatic pressure at the reference fluid depth h_0 and angle with amplitude of rolling angle θ_0. Results corresponding to the resonant excitation frequency are shown in fig. 13(a). The pressure curves show different patterns between the 3 simulations. For the simulation without any baffle, a typical "church roof" profile of the pressure is observed within each rolling cycle. Here, the first peak of pressure represents the impact load due to the wave crest slamming onto the tank wall while the second peak represents the collapse of fluid column. In contrast, no impact loads are observed in the sloshing simulations with either a rigid or an elastic baffle. Maximum pressures of the two cases are much smaller than the previous impact loads, particularly for the case with a rigid baffle. Fig. 13(b) depicts the dimensionless time histories of pressures with an excitation frequency much larger than the resonant frequency. The 3 pressure curves show similar patterns but different maximum values. No impact loads are observed and the static pressures are predominant for the varying pres-

sures for all the 3 cases. Given the slight variation of the fluid level, the pressure peak corresponding to the case without any baffle is really small. In contrast, the pressure peaks corresponding to the cases with baffles are relatively larger, particularly for the case with a rigid baffle. This phenomenon implies that the maximum pressure is not mitigated by the rigid or elastic baffle while the excitation frequency is much larger than the resonate frequency.

According to previous numerical results, the mitigating effects of rigid and elastic baffles on sloshing flows are quite different corresponding to the excitation frequencies of roll motions. Therefore, sloshing behaviors in the 3 series of cases changing with the varying excitation frequencies (ω/ω_0 = 0.61, 0.73, 0.85, 0.91, 0.95, 0.98, 1.01, 1.05, 1.09, 1.11, 1.14, 1.21, 1.27, 1.33, 1.39, 1.47, 1.54, 1.61, 1.67) are further numerically investigated. The simulations of sloshing in a rectangular tank without any baffle are taken as the standard for comparisons for mitigating effects.

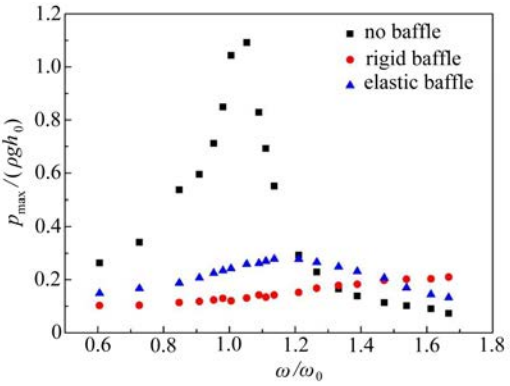

Fig. 14 Averaged maximum impact pressures at P_1 vs. excitation frequencies

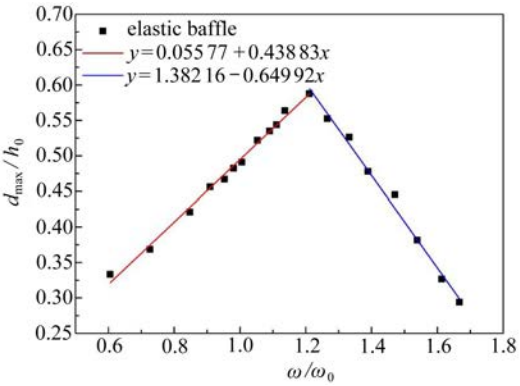

Fig. 15 Averaged maximum displacements at the free end of the elastic baffle vs. excitation frequencies

Fig. 14 shows the statistical results of the maximum pressures of the 3 series of simulations vs. excitation frequencies. Herein, the maximum pressures are calculated based on the mean peaks of time histories corresponding to location P_1. For the sloshing cases without any baffle, increasing the excitation frequency raises the impact loads till frequency $1.05\omega_0$ which is much close to the resonant frequency of the tank. On the contrary, the maximum pressures are gradually reduced with the excitation frequency beyond $1.05\omega_0$. For the rigidly baffled cases, the maximum pressures, on the whole, maintain a relatively low level. Particularly, the peaks of impact loads corresponding to the resonant frequency region are restrained effectively. However, the maximum pressures with excitation frequencies beyond $1.33\omega_0$ are much larger than those in the cases without any baffle. For simulations of series C with an elastic baffle, the maximum pressures rise gently with the excitation frequency till frequency $1.21\omega_0$ which is much larger than the resonant frequency of the tank, and then, cases gradually. Though the pressures at excitation frequencies less than $1.47\omega_0$ maintain a slightly higher level than those of series B, the impact loads due to the resonant phenomenon are also mitigated generally.

Fig. 15 shows the statistical results of the maximum displacements in the case with an elastic baffle vs. excitation frequencies. The displacement is made dimensionless with baffle length h_0. Similar to the calculation of maximum pressures mentioned above, the maximum displacements at the free end of the elastic baffle are calculated based on the mean peaks of time histories. According to this figure, obviously regular distribution of the displacements with the increase of the excitation frequency is observed. The distribution can be fitted in terms of linearly approximate formulas, shown as the ramp-ramp lines with the peak at the frequency $1.21\omega_0$.

3 Conclusions

In this paper, an MPS-FEM coupled method is introduced and a fully Lagrangian FSI solver is implemented by extending the in-house MPS solver MLParticle-SJTU with the FEM module for structure analysis. A partitioned coupling strategy with different time step sizes for fluid and structure analysis is presented. A particle group scheme is considered for the data exchange on the fluid-structure interface, including the application of external fluid forces onto the beam nodes and the deformation of the structural particle model corresponding to the displacements of beam elements. Besides, a particle interaction model is incorporated in the FSI solver, to enhance its performance.

Then, capability of the FSI solver is validated based on the FSI benchmark problem addressed by Antoci et al.[31]. Results of validation show that the numerical shapes of the deformed gate and free surface at different instants are consistent with those of the experiment. The time-varying displacement of the free end of the gate together with the evolution of the water level are in good agreement with the experimental data. In addition, the present FSI solver is applied to the comparative study of the mitigating effects of rigid and elastic baffles on the sloshing motions and impact loads.

Acknowledgments

This work is supported by the National Natural Science Foundation of China (51379125; 51490675; 11432009; 51579145; 11272120); the Chang Jiang Scholars Program of China(T2014099); the Program for Professor of Special Appointment (Eastern Scholar) at Shanghai Institutions of Higher Learning (2013022) and the Innovative Special Project of Numerical Tank of Ministry of Industry and Information Technology of China (2016-23/09), to which the authors are most grateful.

References:

[1] Idelsohn S R, Marti J, Limache A, Onate E. Unified Lagrangian formulation for elastic solids and incompressible fluids: application to fluid-structure interaction problems via the PFEM [J]. *Computer Methods in Applied Mechanics and Engineering*, 2008, **197**(19/20): 1762-1776.

[2] Fossa M, Rizzo C M, Tani G, Viviani M. Simulations of a sloshing experiment by FEM CFD and FEM FSI approaches[C]//*The 22nd International Offshore and Polar Engineering Conference*. Rhodes, Greece, 2012: 530-537.

[3] LIAO Kang-ping, HU Chang-hong. A coupled FDM-FEM method for free surface flow interaction with thin elastic plate[J]. *Journal of Marine Science and Technology*, 2013, **18**(1): 1-11.

[4] Paik K J, Carrica P M. Fluid-structure interaction for an elastic structure interacting with free surface in a rolling tank[J]. *Ocean Engineering*, 2014, **84**: 201-212.

[5] Koshizuka S, Oka Y. Moving particle semi-implicit method for fragmentation of incompressible fluid[J]. *Nuclear Science and Engineering*, 1996, **123**: 421-434.

[6] Khayyer A, Gotoh H. Modified moving particle semi-implicit methods for the prediction of 2D wave impact pressure[J]. *Coastal Engineering*, 2009, **56**(4): 419-440.

[7] Khayyer A, Gotoh H. A higher order Laplacian model for enhancement and stabilization of pressure calculation by the MPS method[J]. *Applied Ocean Research*, 2010, **32**(1): 124-131.

[8] Khayyer A, Gotoh H. Enhancement of stability and accuracy of the moving particle semi-implicit method[J]. *Journal of Computational Physics*, 2011, **230**(8): 3093-3118.

[9] Khayyer A, Gotoh H. A 3D higher order Laplacian model for enhancement and stabilization of pressure calculation in 3D MPS-based simulations[J]. *Applied Ocean Research*, 2012, **37**: 120-126.

[10] Kondo M, Koshizuka S. Improvement of stability in moving particle semi-implicit method[J]. *International Journal for Numerical Methods in Fluids*, 2011, **65**(6): 638-654.

[11] Tanaka M, Masunaga T. Stabilization and smoothing of pressure in MPS method by quasi-compressibility[J]. *Journal of Computational Physics*, 2010, **229**(11): 4279-4290.

[12] Ikari H, Khayyer A, Gotoh H. Corrected higher order Laplacian for enhancement of pressure calculation by projection-based particle methods with applications in ocean engineering[J]. *Journal of Ocean Engineering and Marine Energy*, 2015, **1**(4): 361-376.

[13] Mitsume N, Yoshimura S, Murotani K, Yamada T. MPS-FEM partitioned coupling approach for fluid-structure interaction with free surface flow[J]. *International Journal of Computational Methods*, 2014, **11**(4): 4157-4160.

[14] Mitsume N, Yoshimura S, Murotani K, Yamada T. Improved MPS-FE fluid-structure interaction coupled method with MPS polygon wall boundary model[J]. *Computer Modeling in Engineering and Sciences*, 2014, **101**(4): 229-247.

[15] Hwang S C, Khayyer A, Gotoh H, Park J C. Development of a fully Lagrangian MPS-based coupled method for simulation of fluid-structure interaction problems[J]. *Journal of Fluids and Structures*, 2014, **50**: 497-511.

[16] Hwang S C, Park J C, Gotoh H, Khayyer A, Kang K J. Numerical simulations of sloshing flows with elastic baffles by using a particle-based fluid-structure interaction analysis method [J]. *Ocean Engineering*, 2016, **118**: 227-241.

[17] Sun Z, Xing J T, Djidjeli K, Cheng F. Coupling MPS and modal superposition method for flexible wedge dropping simulation[C]//*The Twenty-fifth International Ocean and Polar Engineering Conference*. Kona, Hawaii, USA, 2015:144-151.

[18] Hou G, Wang J, Layton A. Numerical methods for fluid-structure interaction—a review[J]. *Communications in Computational Physics*, 2012, **12**(2): 337-377.

[19] Longatte E, Verremana V, Souli M. Time marching for simulation of fluid-structure interaction

problems[J]. *Journal of Fluids and Structures*, 2009, **25**(1): 95-111.

[20] Heil M, Hazel A L, Boyle J. Solvers for large-displacement fluid-structure interaction problems: segregated versus monolithic approaches[J]. *Computational Mechanics*, 2008, **43**(1): 91-101.

[21] Zhang Y L, Tang Z Y, Wan D C. Numerical investigations of waves interacting with free rolling body by modified MPS method[J]. *International Journal of Computational Methods*, 2016, **13**(4): 1641013.

[22] Tang Z Y, Zhang Y L, Wan D C. Multi-resolution MPS method for free surface flows[J]. *International Journal of Computational Methods*, 2016, **13**(4): 1641018.

[23] Tang Z Y, Zhang Y L, Wan D C. Numerical simulation of 3D free surface flows by overlapping MPS[J]. *Journal of Hydrodynamics*, 2016, **28**(2): 306-312.

[24] Tang Z Y, Wan D C, Chen G, Xiao Q. Numerical simulation of 3D violent free surface flows by multi-resolution MPS method[J]. *Journal of Ocean Engineering and Marine Energy*, 2016, **2**(3): 355-364.

[25] Tang Z Y, Wan D C. Numerical simulation of impinging jet flows by modified MPS method [J]. *Engineering Computations*, 2015, **32**(4): 1153-1171.

[26] Zhang Y X, Wan D C, Hino T. Comparative study of MPS method and level-set method for sloshing flows[J]. *Journal of Hydrodynamics*, 2014, **26**(4): 577-585.

[27] Koshizuka S, Nobe A, Oka Y. Numerical analysis of breaking waves using the moving particle semi-implicit method[J]. *International Journal for Numerical Methods in Fluids*, 1998, **26**(7): 751-769.

[28] Lee B H, Park J C, Kim M H, Hwang S C. Step-by-step improvement of MPS method in simulating violent free-surface motions and impact-loads[J]. *Computer Methods in Applied Mechanics and Engineering*, 2011, **200**(9/12): 1113-1125.

[29] Newmark N M. A method of computation for structural dynamics[J]. *Journal of the Engineering Mechanics Division*, 1959, **85**: 67-94.

[30] Hsiao K M, Lin J Y, Lin W Y. A consistent co-rotational finite element formulation for geometrically nonlinear dynamic analysis of 3-D beams[J]. *Computer Methods in Applied Mechanics and Engineering*, 1999, **169**(1/2): 1-18.

[31] Antoci C, Gallati M, Sibilla S. Numerical simulation of fluid-structure interaction by SPH[J]. *Computers and Structures*, 2007, **85**(11/14): 879-890.

基于 MPS-FEM 耦合方法对比研究刚性与弹性挡板对液舱晃荡的抑制作用

张友林， 陈 翔， 万德成

（海洋工程国家重点实验室(上海交通大学)；
上海交通大学 船舶海洋与建筑工程学院；高新船舶与深海开发装备协同创新中心，上海 200240）

摘要： 由流体冲击载荷引起的流固耦合问题广泛存在于船舶与海洋工程领域.例如:在特定激励频率下载液货舱内流体的非线性运动引起对舱壁的砰击作用,进而可能影响液舱围护系统的安全性.由于此类流固耦合问题通常涉及多学科知识,且流体自由面的变化具有强非线性特征,对研究人员带来较大挑战.考虑到 Lagrange 类方法在处理结构和流体自由面大变形问题上的优势,基于 MPS-FEM 耦合方法开发了流固耦合求解器.其中,采用 MPS 方法来数值模拟流体场瞬态变化,FEM 方法来分析结构场的变形问题.此外,该求解器采用了弱耦合的方式来实现流体场和结构场之间的数据传递.为了验证该方法在处理流固耦合问题上的可靠性,首先数值研究了溃坝泄洪流与弹性挡板之间的流固耦合标准算例,数值结果与实验标准结果能够较好地吻合.此后,采用该求解器数值研究了带刚性挡板和弹性挡板的液舱晃荡问题,对比分析了多种激励频率下两种挡板对液舱内流体运动及舱壁上冲击压力的抑制效果.

关 键 词： 粒子法； 半隐式移动粒子法（MPS）； 有限单元法（FEM）； 流固耦合(FSI)；液舱晃荡； 溃坝流； MLParticle-SJTU 求解器

基金项目： 国家自然科学基金(51379125；51490675；11432009；51579145；11272120)；长江学者奖励计划(T2014099)

引用本文/Cite this paper：

ZHANG You-lin, CHEN Xiang, WAN De-cheng. An MPS-FEM coupled method for the comparative study of liquid sloshing flows interacting with rigid and elastic baffles[J]. *Applied Mathematics and Mechanics*, 2016, **37**(12): 1359-1377.

张友林, 陈翔, 万德成. 基于 MPS-FEM 耦合方法对比研究刚性与弹性挡板对液舱晃荡的抑制作用[J]. 应用数学和力学, 2016, **37**(12): 1359-1377.